Sensors

International Edition: DOI: 10.1002/anie.201604431
German Edition: DOI: 10.1002/ange.201604431

Wireless Hazard Badges to Detect Nerve-Agent Simulants

*Rong Zhu[+], Joseph M. Azzarelli[+], and Timothy M. Swager**

Abstract: *Human exposure to hazardous chemicals can have adverse short- and long-term health effects. In this Communication, we have developed a single-use wearable hazard badge that dosimetrically detects diethylchlorophosphate (DCP), a model organophosphorous cholinesterase inhibitor simulant. Improved chemically actuated resonant devices (CARDs) are fabricated in a single step and unambiguously relate changes in chemiresistance to a wireless readout. To provide selective and readily manufacturable sensor elements for this platform, we developed an ionic-liquid-mediated single walled carbon nanotube based chemidosimetric scheme with DCP limits of detection of 28 ppb. As a practical demonstration, an 8 h workday time weighted average equivalent exposure of 10 ppb DCP effects an irreversible change in smartphone readout.*

Human exposure to hazardous chemicals in the environment, in the workplace, or in military contexts remains a critical human health concern. Furthermore, recent and continued human exposure to hazardous chemicals in "everyday" environments has prompted heightened interest in chemical monitoring by citizens.[1,2] Most toxic gases are not visually detectable and can be harmful at persistent exposures below the human olfaction threshold. The ability to quantify a chemical hazard dose in a temporally correlated fashion would enable real-time personalized risk assessment (Figure 1 a).

Real-time, personalized situational awareness remains impractical for all but the most specialized applications: existing technological solutions are largely limited to colorimetric reagent tests such as Dräger tubes,[3] various electronic nose technologies,[4] and scaled-down spectroscopy-based methods.[5] The principal limitations of these techniques are either cost, reliability, sensitivity, ease-of-use, physical size, power requirements, or all of the above. As a result, personal chemical dosimeters have not been broadly implemented. To address this need, we have developed a low-cost, user-friendly, passive, reliable chemical hazard badge that collects actionable health risk data that can be transmitted wirelessly to cloud data storage.

Our concept was to create wearable, battery-free, single-use chemical hazard badges that cost less than $1, are combustible or recyclable and therefore environmentally friendly, and are smartphone-communicable (Figure 1 b). Passive radio frequency communication devices, such as near field communication (NFC) tags, meet these requirements.[6]

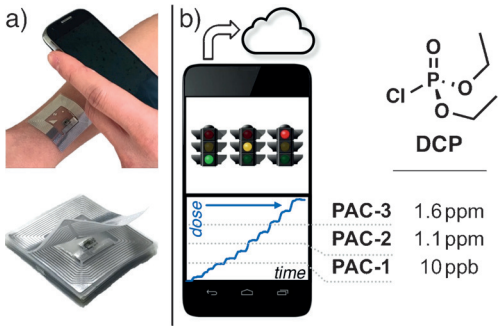

Figure 1. a) A wearable, passive, disposable chemical dosimeter hazard badge can be scanned periodically throughout the day. A fresh tag would be peeled off from a pack at the beginning of each time period. b) Quantification of the "dose" of the hazardous chemical using a smartphone enables facile information collection to a centralized database, by means of cloud data transfer/storage. Standardized decisions can be informed by predefined protective action criteria (PAC) levels associated with equivalent exposure time weighted average hazardous chemical concentration.

We targeted diethyl chlorophosphate (DCP) in our development of a prototype chemical hazard dosimeter. DCP has been studied as a target analyte for chemical sensors mainly as a chemical warfare nerve agent (NA) simulant.[7] It is also a chemical analogue of cholinesterase inhibiting organophosphate pesticides.[8] For chemical hazards like DCP, time-weighted-average (TWA) permissible exposure limits are the most relevant parameter in dictating the necessity and type of protective actions to be taken.

Ideal chemical hazard dosimeters enable the instantaneous assessment of a TWA exposure based on temporally correlated chemical dose information. For instance, the US Department of Energy has established "protective action criteria" levels (PAC) for over 3000 hazardous substances, including DCP.[9] Accordingly, hazard badges could be designed to activate at dosage levels that induce mild, transient health effects (PAC-1), irreversible or other serious health effects that could inhibit the ability to further protect oneself (PAC-2), or life threatening health effects (PAC-3). Furthermore, personal exposure information could be synchronized with a cloud database[6] to expose spatiotemporal trends[10] and enable emergency decision making by a second party in the case of incapacitation of the hazard badge wearer.

We have previously demonstrated that two-step conversion of NFC tags into chemically actuated resonant devices

[*] Dr. R. Zhu,[+] J. M. Azzarelli,[+] Prof. Dr. T. M. Swager
Department of Chemistry and Institute for Soldier Nanotechnologies
Massachusetts Institute of Technology
Cambridge, MA (USA)
E-mail: tswager@mit.edu
[+] These authors contributed equally to this work. The author order was determined by coin toss.
Supporting information and the ORCID identification number(s) for the author(s) of this article can be found under http://dx.doi.org/10.1002/anie.201604431.

(CARDs) can enable semiquantitative, selective detection of chemical gases with a smartphone.[11] However, ultra-trace (less than part-per-million) sensing and dosimetric detection remain challenging with our initial designs.[12] To address these challenges we report herein key improvements to both the circuit design as well as new single walled carbon nanotube (SWCNT)-based chemiresistive dosimetric materials.

In our first generation CARD platform (*series*-CARD, or *s*-CARD), the chemiresistor (R_s) is incorporated in series with the NFC integrated circuit (IC) in a two-step method. This method involves the disruption and recompletion of the circuit (Figure 2a). The raw chemical information that the chemiresistor collects is converted and wirelessly transmitted, mainly in the form of device resonant frequency (f_0) amplitude, or gain (in dB).

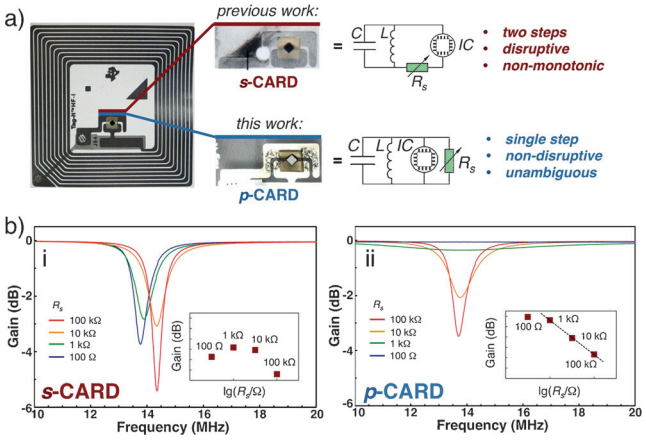

Figure 2. a) Single-step nondisruptive conversion of a commercial NFC tag to a *p*-CARD and comparison to our first-generation design. To create an *s*-CARD, a hole is punched removing some of the aluminum lead material and disrupting the circuit, which is reconnected by the chemiresistor. To create a *p*-CARD, the material is deposited on the aluminum leads connecting the IC. Note that the *p*-CARD photograph has opposite contrast (aluminum metal is bright) to reveal the deposited chemiresistor. b) Resonance-frequency traces for s-CARD (i) and *p*-CARD (ii) with varying R_s. Respective gain values measured for each R_s (insets in (i) and (ii)).

Although the *s*-CARD proved successful in selectively detecting chemically diverse analytes at parts-per-million (ppm) levels, we noticed that its circuit structure could introduce physical constraints to the response magnitude corresponding to a certain change in the sensor resistance (ΔGain/ΔR_s). We have systematically examined the gain readout of a series of *s*-CARDs with fixed resistors (R_s) in place of chemiresistors. These resistors ranged from 100 Ω to 100 kΩ, which encompassed the typical dynamic range of our CNT-based chemiresistors (1 kΩ to 100 kΩ). As shown in Figure 2b (part (i)), the device resonated in all cases, and a non-monotonic change in the gain readout was observed as R_s increased (Figure 2b, inset in part (i)). This resulted in a minimal gain difference observed between $R_s = 1$ kΩ and 10 kΩ. More importantly, the non-monotonicity leads to ambiguous results when the device is operating within a large dynamic gain range.

We hypothesized that incorporation of the chemiresistor in parallel with the integrated circuit would serve to overcome the drawbacks associated with *s*-CARDs. Such a modification process produced a new type of CARD platform: *parallel*-CARD, or *p*-CARD. For a proof of concept, parallel fixed resistors ranging from 100 Ω to 100 kΩ were used to construct a series of *p*-CARDs. Their gain readouts were measured. As shown in Figure 2b (part (ii)), as R_s increased, the device underwent a monotonic decrease in gain and proceeded from nonresonant to resonant. The gain–logR_s relationship was linear from 1 kΩ through 100 kΩ (Figure 2b, inset in part (ii)).

The importance of practicability in the fabrication procedure of a new device structure should not be understated. In this regard, the *p*-CARD design is advantageous; it does not require disruption of the existing radio frequency ID (RFID) circuit and can be fabricated in a single step. The *p*-CARD is created by simple deposition of chemiresistive material between the leads connecting the IC (Figure 2a). This nondisruptive modification method not only results in more consistent device performance but also makes *p*-CARDs amenable to inkjet printing and roll-to-roll manufacturing processes.[13]

With the *p*-CARD platform in hand, we turned our attention to the development of a DCP-responsive dosimetric SWCNT chemiresistor[14] based on the irreversible hydrolysis of DCP.[15] To enhance the response by accelerating hydrolysis, we targeted SWCNTs in ionic liquids.[16] In addition to creating solution-phase reactivity at the SWCNT surface, ionic liquids (IL) have been shown to partially debundle SWCNTs when the two components are ground together in the solid state or when a mixture of SWCNTs and an IL are sonicated together in the presence of cosolvents.[17] Despite these advantages, SWCNT/ILs are not an established chemiresistor platform.[18]

We initially tested the response of *p*-CARDs fabricated with SWCNT/IL composites to DCP in nitrogen (N_2). We found that a combination of SWCNT and 1-butyl-3-methylimidazolium chloride (BMIMCl) showed a good, irreversible response. Previous work in our laboratory has shown that small-molecule selectors incorporated into chemiresistor formulations can selectively enhance the resistive response to gas analytes.[19] By incorporating 2-(2-hydroxy-1,1,1,3,3,3-hexafluoropropyl)-1-naphthol (HFIPN) as a hydrogen-bonding chelator/catalyst[20] into the mixture, a 3.3-times improvement in response to DCP was realized (Figure 3a).

The irreversible response and significant enhancement associated with the BMIMCl/HFIPN-based chemiresistor was consistent with observed hydrolysis kinetics of DCP in solution (Scheme 1). We found that at room temperature, DCP undergoes only minor hydrolysis after stirring in CD_3CN for 10 min, even in the presence of excess water (8 equiv) as monitored by ^{31}P NMR spectroscopy (Scheme 1, conditions ii: for DCP $\delta \approx 4.8$ ppm). In contrast, when DCP was added to a mixture of HFIPN and BMIMCl (a minimal amount of CD_3CN was added to obtain a liquid mixture) in the absence of any additional water, instantaneous hydrolysis occurred with the trace water present under an ambient atmosphere (conditions i). Specifically, a significant portion

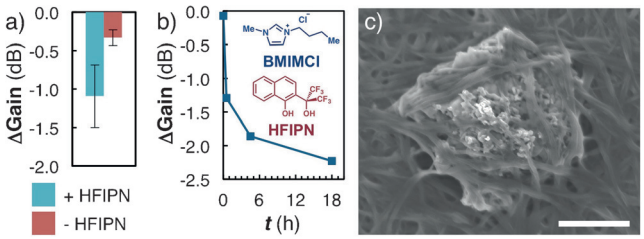

Figure 3. a) When exposed to DCP (1 ppm) for 50 s, *p*-CARDs fabricated with HFIPN (blue bar, left) had a 3.3-times larger magnitude of response than those fabricated without HFIPN (red bar, right). b) Magnitude of response (ΔGain) as a function of device "age". Blue squares represent different devices. The structures of the components of the optimized system are shown (inset). c) SEM image of a typical SWCNT-wrapped microcrystal. Scale bar = 1 μm.

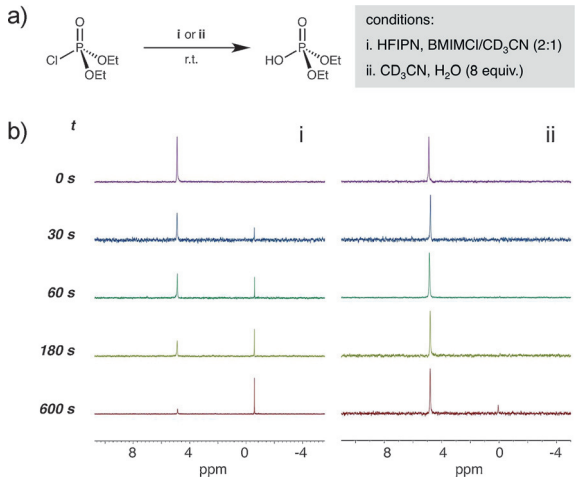

Scheme 1. ^{31}P NMR spectroscopy kinetics study of DCP hydrolysis.

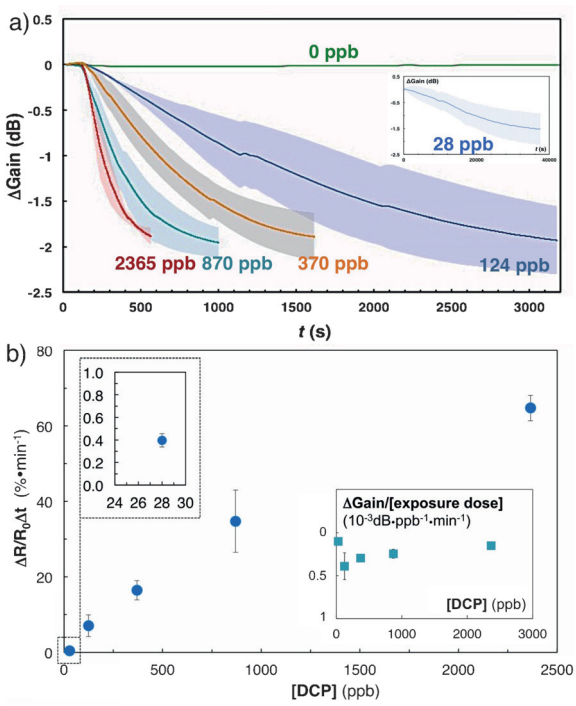

Figure 4. *p*-CARD DCP dosimeter performance with varying DCP concentrations: a) Saturation plots. DCP exposure started at 100 s. The results are the averages of multiple individual devices tested (X = 5, except for [DCP] = 28 ppb (inset) where X = 3). Shaded areas indicate standard deviations. b) Relative resistance changes per minute. The upper inset shows the expanded portion for [DCP] = 28 ppb. The lower inset shows the exposure-dose-normalized response determined for *p*-CARDs at each concentration tested.

was hydrolyzed within a few seconds, indicated by the emerging signal for diethylphosphoric acid at $\delta \approx -0.5$ ppm. Nearly full conversion was observed within 10 min.

Upon a more thorough investigation, we observed that there was a maturing process with the SWCNT/BMIMCl system, accompanied by two coinciding observations: 1) the *p*-CARD baseline (gain) drift was effectively zero and 2) the magnitude of the response to DCP increased substantially as a function of time, reaching a maximum after about 18 h (Figure 3b). Visual inspection and optical microscopy confirm time-dependent crystallization of BMIMCl at the surface of *p*-CARD (Figure S7). Scanning electron microscopy (SEM) revealed the formation of SWCNT-wrapped microcrystal structures (Figure 3c). We hypothesized that such structures could increase SWCNT surface area and thus lead to an enhanced response. This is consistent with our observation that *p*-CARDs fabricated with 1-butyl-3-methylimidazolium type ILs that are liquids at room temperature (anion = hexafluorophosphate, bromide, or iodide) did not demonstrate this behavior. Recent reports suggest solid-phase ILs hold promise as a tunable class of materials for a broad array of applications.[21]

With the optimized system in hand, we next evaluated its performance toward various concentrations of DCP. We fabricated a series of *p*-CARDs that incorporated the BMIMCl/HFIPN/SWCNT-based chemiresistor. The individual device was exposed to a nitrogen flow for 100 s followed by DCP vapor until its gain readout reached saturation. The results are summarized in Figure 4a.

Consistent magnitudes of saturation response were observed ($\Delta\text{Gain} \approx -1.9$ dB, or $\Delta R/R_0 \approx 1400\,\%$) when the DCP concentration was greater than 100 parts-per-billion (ppb), whereas a slightly diminished overall change in gain was obtained with 28 ppb DCP ($\Delta\text{Gain} \approx -1.5$ dB; see Figure 4a, inset). From the linear region of the saturation plots, we were able to extract the relative sensor resistance change per minute as a benchmark for detection sensitivity evaluation (Figure 4b). It was found that R_s increased by over 60 % after exposure to 2.4 ppm DCP for only 1 min. This high sensitivity and fast response kinetics allowed the detection of DCP at a concentration as low as 28 ppb and on a practical time scale (0.4 % min^{-1}).

A true test of a dosimeter is based on the response behavior across all combinations of time and concentration. Ideally the response of a dosimeter is proportional to the exposure dose, the product of analyte concentration, and exposure time ([analyte]·Δ*t*). It was determined across three orders of concentration magnitude that the exposure-dose-normalized response (gain) of all *p*-CARDs tested fell within a relatively narrow range (Figure 4b, lower inset), indicating

concentration-independent dosimetry of our optimized system. By taking the average exposure-dose-normalized response, theATT="tpl=0mm tpr=0mm tptxpt=4.8mm tptxt=5.2mm tptxb=4.2mm" exposure-dose-dependent relationship to the change in gain of a *p*-CARD can be empirically derived as:

$$\Delta\text{Gain} = A\int_{t_1}^{t_2}[\text{DCP}]dt \qquad (1)$$

Where $A = -(2.5 \pm 1.2) \times 10^{-4}$ dB ppb^{-1} min^{-1} and t is measured in minutes. This key relationship thus enables unambiguous equivalent exposure assessments based on the relative change in gain. Furthermore, when combined with knowledge of the power threshold of binary *p*-CARDs, preprogrammed *p*-CARDs that switch on and off after passing a predefined equivalent exposure threshold can be easily and predictably fabricated.

Next, the NA-simulant-triggered smartphone binary switch of this system was demonstrated wherein a *p*-CARD was repeatedly exposed to DCP vapor (2 ppm) for 50 s followed by 170 s N_2 (Figure 5). The device was designed to switch on when it had exceeded a PAC-1 threshold. Initially, the *p*-CARD was below the smartphone's on/off threshold at gain = −0.225 dB, and thus was unreadable ("off" state, indicated by green dots). The corresponding frequency-gain plot of this device ($t = 0$ s) was nearly flat, demonstrating poor device resonance within the working frequency region of the NFC reader (see Figure S9 in the Supporting Information).

As the device was iteratively exposed to DCP: 1) a consistent irreversible gain readout decrease (R increase) was observed, as showcased by the staircase-shape plot; 2) the resonance amplitude of the device increased, as indicated by the increasing depth of the minima in the frequency–gain plot; 3) After 3 cycles, corresponding to a PAC-1 TWA of 10 ppb, the device's resonance amplitude exceeded the readability threshold and became readable by the smartphone (state "on", indicated by red dots).[22]

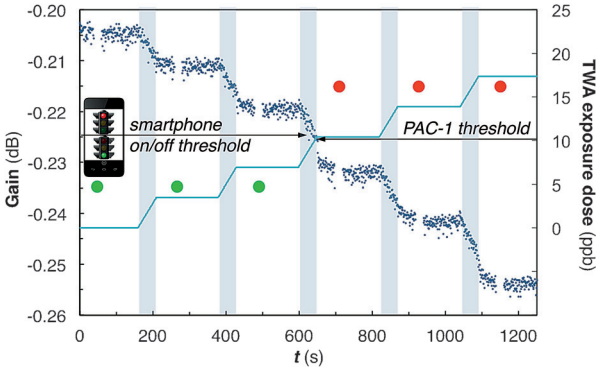

Figure 5. *p*-CARD DCP PAC-1 dosimeter. A *p*-CARD's gain (left axis, blue data points) was measured while it was iteratively exposed to DCP (2 ppm in N_2; shaded bars). The equivalent exposure TWA (right axis, blue line) was calculated, and the *p*-CARD was read by a smartphone once per cycle. Below the PAC-1 threshold, the *p*-CARD is unreadable (green dots). Above the PAC-1 threshold, the *p*-CARD becomes readable (red dots).

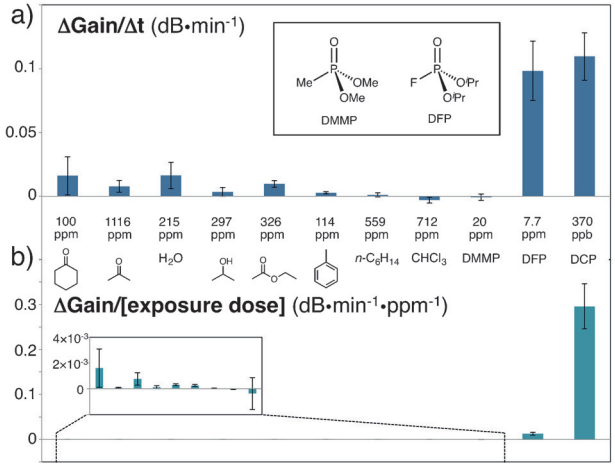

Figure 6. Selectivity of *p*-CARD DCP dosimeter towards interferents. Change in *p*-CARD gain as a function of a) exposure time (min) and b) exposure dose (min ppm).

When it comes to in-field chemical hazard dosimetry, chemiresistor selectivity to the target analyte over commonly encountered interferent chemicals is critical for minimizing the occurrence of false alarms.[23] Toward this end, a series of potential interferent chemicals were evaluated. Overall, the responses (ΔGain/Δt) of our *p*-CARD DCP dosimeter toward NA simulants (DCP and diisopropyl fluorophosphates (DFP)) at ppb or low-ppm level were at least one order of magnitude larger than those resulted from the highly concentrated vapors (about 100–1000 ppm) of the interferents studied (Figure 6a). This good selectivity can be better characterized by the exposure-dose-normalized responses (Figure 6b). Among the interferents tested, ketone, ester, or hydroxy functional group containing compounds afforded a detectable sensor resistance increase, presumably through hydrogen-bonding. Hydrocarbon/halogenated hydrocarbons were essentially inert to the sensor.[24] Dimethyl methylphosphonate (DMMP), a hydrogen-bond-accepting NA simulant that does not react covalently under these conditions, elicited a much smaller response than DCP and DFP at comparable concentrations, which is consistent with the irreversible hydrolysis proposed for the response to DCP and DFP.[25]

In conclusion, we have developed a highly sensitive and selective disposable wireless dosimetric chemical hazard badge that can reliably detect NA simulants down to 28 ppb. This was enabled by 1) the invention of a new wirelessly addressable sensor platform, *p*-CARD, derived from commercial NFC tags in a single step, and 2) the identification of a SWCNT/IL-based chemiresistor that selectively responds to the target analyte through instantaneous irreversible reactions. This badge allows the quantification of chemical hazard dose in a temporally correlated fashion and transmission of that information wirelessly, which has been demonstrated by the smartphone readability switch upon repeated exposures. The consistent dosimetric behavior of this system enables real-time hazard assessment that is relevant to widely employed chemical hazard regulation standards.

Acknowledgements

The authors would like to acknowledge the financial support of the Chemical and Biological Technologies Department at the Defense Threat Reduction Agency (DTRA-CB) via Grant BA12PHM123 in the "Dynamic Multifunctional Materials for a Second Skin D[MS]2" program, and the Army Research Office through the Institute for Soldier Nanotechnologies. We thank Marshall Craft (MIT) for building our VNA trace analysis LabView program and assisting in 3D printing of a gas sensing enclosure, Dr. Steven Kooi for assisting in 3D printing of a gas sensing enclosure, Dr. Fei Yan (MIT) for discussion, and Vera Schroeder (MIT) for 3D graphic design.

Keywords: carbon nanotubes · dosimeter · ionic liquids · nerve agents · sensors

How to cite: *Angew. Chem. Int. Ed.* **2016**, *55*, 9662–9666
Angew. Chem. **2016**, *128*, 9814–9818

[1] a) D. Vallero *Fundamentals of Air Pollution*, 5th ed., Elsevier, Waltham, **2014**, pp. 139–378; b) S. Steinle, S. Reis, C. E. Sabel, *Sci. Total Environ.* **2013**, *443*, 184–193; c) A. Vale, T. C. Marrs, P. Rice, *Medicine* **2012**, *91*, 106–108; d) B. Erickson, *Chem. Eng. News* **2016**, *94*, 30–34.

[2] R. P. Pohanish, *Sittig's Handbook of Toxic and Hazardous Chemicals and Carcinogens*, 6th ed., Elsevier Science, Burlington, **2011**.

[3] *Dräger-Tubes & CMS-Handbook Soil, Water, and Air Investigations as Well as Technical Gas Analysis*, 16th ed., Dräger Safety AG & Co., Lubeck, **2001**.

[4] A. D. Wilson, M. Baietto, *Sensors* **2009**, *9*, 5099–5148.

[5] R. Sferopoulos, *Human Protection and Performance Division*, Commonw. Aust., Victoria, **2008**, DSTO-GD-0570.

[6] V. Coskun, B. Ozdenizci, K. Ok, *Wirel. Pers. Commun.* **2013**, *71*, 2259–2294.

[7] For selected recent examples, see: a) X. Zhou, Y. Zeng, C. Liyan, X. Wu, J. Yoon, *Angew. Chem. Int. Ed.* **2016**, *55*, 4729–4733; *Angew. Chem.* **2016**, *128*, 4807–4811; b) C. Belger, J. G. Weis, E. Egap, T. M. Swager, *Macromolecules* **2015**, *48*, 7990–7994; c) Z. Lei, Y. Yang, *J. Am. Chem. Soc.* **2014**, *136*, 6594–6597; d) H. J. Kim, J. H. Lee, H. Lee, J. H. Lee, J. H. Lee, J. H. Jung, J. S. Kim, *Adv. Funct. Mater.* **2011**, *21*, 4035–4040; e) S.-W. Zhang, T. M. Swager, *J. Am. Chem. Soc.* **2003**, *125*, 3420–3421.

[8] *Toxicology of Organophosphate & Carbamate Compounds*, (Ed.: R. C. Gupta), Elsevier, Burlington, **2006**, pp. 103–160; pp. 209–217; pp. 599–655.

[9] a) *Temporary Emergency Exposure Limits for Chemicals: Methods and Practice*, U. S. Dept. Energ., Washington, D.C., **2008**, DOE-HDBK-1046-2008; b) *Protective Action Criteria Rev. 28A Table 2*, U.S. Dept. Energ. Subcomittee on Consequence Assessment and Protective Actions (SCAPA).

[10] N. Cressie, C. K. Wilke in *Statistics for Spatio-Temporal Data*, Wiley, Hoboken, **2011**, pp. 243–356.

[11] J. M. Azzarelli, K. A. Mirica, J. B. Ravnsbæk, T. M. Swager, *Proc. Natl. Acad. Sci. USA* **2014**, *111*, 18162–18166.

[12] a) S. Goswami, S. Das, K. Aich, *RSC Adv.* **2015**, *5*, 28996–29001; b) A. M. Costero, M. Parra, S. Gil, R. Gotor, R. Martínez-Mañez, F. Sancenón, S. Royo, *Eur. J. Org. Chem.* **2012**, 4937–4946.

[13] a) L. Yang, R. Zhang, D. Staiculescu, C. P. Wong, M. M. Tentzeris, *IEEE Antennas Wirel. Propag. Lett.* **2009**, *8*, 653–656; b) K. Kordas, T. Mustonen, G. Toth, H. Jantunen, M. Lajunen, C. Soldano, S. Talapatra, S. Kar, R. Vajtai, P. M. Ajayan, *Small* **2006**, *2*, 1021–1025; c) R. A. Potyrailo, A. Burns, C. Surman, D. J. Lee, E. McGinniss, *Analyst* **2012**, *137*, 2777–2781; d) W. Lee, H. Koo, J. Sun, J. Noh, K.-S. Kwon, C. Yeom, Y. Choi, K. Chen, A. Javey, G. Cho, *Sci. Rep.* **2015**, *5*, 17707; e) M. Jung, J. Kim, J. Noh, N. Lim, C. Lim, G. Lee, J. Kim, H. Kang, K. Jung, A. D. Leonard, et al., *IEEE Trans. Electron Devices* **2010**, *57*, 571–580.

[14] J. F. Fennell, S. F. Liu, J. M. Azzarelli, J. G. Weis, S. Rochat, K. A. Mirica, J. B. Ravnsbæk, T. M. Swager, *Angew. Chem. Int. Ed.* **2015**, *54*, 1266–1269; *Angew. Chem.* **2015**, *127*, 1282–1285.

[15] a) K. Kim, O. G. Tsay, D. A. Atwood, D. G. Churchill, *Chem. Rev.* **2011**, *111*, 5345–5403; b) S.-Y. Moon, Y. Liu, J. T. Hupp, O. K. Farha, *Angew. Chem. Int. Ed.* **2015**, *54*, 6795–6799; *Angew. Chem.* **2015**, *127*, 6899–6903; c) E. López-Maya, C. Montoro, L. M. Rodríguez-Albelo, S. D. A. Cervantes, A. A. Lozano-Pérez, J. L. Cenís, E. Barea, J. A. R. Navarro, *Angew. Chem. Int. Ed.* **2015**, *54*, 6790–6794; *Angew. Chem.* **2015**, *127*, 6894–6898; d) H. Sohn, S. Létant, M. J. Sailor, W. C. Trogler, *J. Am. Chem. Soc.* **2000**, *122*, 5399–5400.

[16] a) T. Welton, *Chem. Rev.* **1999**, *99*, 2071–2083; b) P. Pavez, D. Millán, C. Cocq, J. G. Santos, F. Nome, *New J. Chem.* **2015**, *39*, 1953–1959; c) P. Pavez, D. Millán, C. J. I. Morales, E. A. Castro, C. López A., J. G. Santos, *J. Org. Chem.* **2013**, *78*, 9670–9676.

[17] a) T. Fukushima, A. Kosaka, Y. Ishimura, T. Yamamoto, T. Takigawa, N. Ishii, T. Aida, *Science* **2003**, *300*, 2072–2074; b) T. Fukushima, T. Aida, *Chem. Eur. J.* **2007**, *13*, 5048–5058; c) S. Zhang, Q, Zhang, Y. Zhang, Z. Chen, M. Watanabe, Y. Deng, *Prog. Mater. Sci.* **2016**, *77*, 80–124; d) M. Tunckol, J. Durand, P. Serp, *Carbon* **2012**, *50*, 4303–4334.

[18] For a graphene–IL-based quartz crystal microbalance gas sensor, see: a) Q. Ji, I. Honma, S.-M. Paek, M. Akada, J. P. Hill, A. Vinu, K. Ariga, *Angew. Chem. Int. Ed.* **2010**, *49*, 9737–9739; *Angew. Chem.* **2010**, *122*, 9931–9933; A SWCNT–IL hybrid has been used as electrode material for voltammetric sensing: b) S. Fan, F. Xiao, L. Liu, F. Zhao, B. Zeng, *Sens. Actuators B* **2008**, *132*, 34–39.

[19] K. A. Mirica, J. M. Azzarelli, J. G. Weis, J. M. Schnorr, T. M. Swager, *Proc. Natl. Acad. Sci. USA* **2013**, *110*, E3265–E3270.

[20] a) F. Wang, T. M. Swager, *J. Am. Chem. Soc.* **2011**, *133*, 11181–11193; b) J.-P. Bégué, D. Bonnet-Delpon, B. Crousse, *Synlett* **2004**, 18–29.

[21] I. M. Warner, B. El-zahab, N. Siraj, *Anal. Chem.* **2014**, *86*, 7184–7191.

[22] While we demonstrated the binary switch with the commercial NFC tags that have a threshold around −0.2 dB, we also devised a simple method to customize this parameter, which is described in the Supporting Information.

[23] Y. Seto, M. Kanamori-Kataoka, K. Tsuge, I. Ohsawa, K. Matsushita, H. Sekiguchi, T. Itoi, K. Iura, Y. Sano, S. Yamashiro, *Sens. Actuators B* **2005**, *108*, 193–197.

[24] We noted that ammonia vapor led to sensor resistance decrease, which is likely due to a deprotonation process.

[25] *p*-CARDs did not respond significantly to low concentrations of water vapor (< 10% relative humidity) and the response to DCP was not significantly affected under such a level of humidity. However, a continuous flow (0.5–1.5 L min^{-1}) of moisture vapor of elevated humidity (30% to 100% of the saturation humidity) could compromise the sensor. For details see the Supporting Information.

Received: May 10, 2016
Published online: July 6, 2016

